



Removal of azo dye from aqueous solution by host–guest interaction with β -cyclodextrin

Ke-Deng Zhang^a, Fang-Chang Tsai^{a,*}, Ning Ma^a, Yue Xia^a, Huan-Li Liu^a, Xuan Guo^a, Xiao-Yan Yu^a, Tao Jiang^a, Tai-Chin Chiang^{b,c}, Chang-Jung Chang^d

^aHubei Key Laboratory of Polymer Materials, Key Laboratory for the Green Preparation and Application of Functional Materials (Ministry of Education), Hubei Collaborative Innovation Center for Advanced Organic Chemical Materials, School of Materials Science and Engineering, Hubei University, 368 Youyi Avenue, Wuchang, Wuhan 430062, China, Tel./Fax: +86 2788661729; emails: tfc0323@gmail.com (F.-C. Tsai), zkd19910705@hotmail.com (K.-D. Zhang), maning@whu.edu.cn (N. Ma), xia.yue1990@hotmail.com (Y. Xia), pangchoudan521@163.com (H.-L. Liu), 514620157@qq.com (X. Guo), 1351212063@qq.com (X.-Y. Yu), jiangtao@hubu.edu.cn (T. Jiang)

^bDepartment of Materials Science and Engineering, National Taiwan University of Science and Technology, 43, Sec. 4, Keelung Road, Da'an Dist., Taipei 10607, Taiwan, ROC, email: tcchiang0102@gmail.com

^cDepartment of Materials Science and Engineering, Tokyo Institute of Technology, 2-12-1-S8-32, O-okayama, Meguro-ku, Tokyo 152-8552, Japan

^dMaterial and Chemical Research Laboratories, Industrial Technology Research Institute, 195, Sec. 4, Chung Hsing Road, Chutung, Hsinchu 31040, Taiwan, ROC, email: changcj@itri.org.tw

Received 10 January 2017; Accepted 7 July 2017

ABSTRACT

Water pollution is a serious threat to the human beings' survival and development and a universal problem across community society. In this work, a novel β -cyclodextrin (β -CD) hydrogel was successfully synthesized by polycondensation reaction using epichlorohydrin (EPI) and β -CD under basic condition, and the swelling ratio at room temperature was up to 181%. The adsorption behavior and adsorption mechanism of EPI crosslinked β -CD were evaluated by using acid orange 7 (AO7) as a model dye. We found that the adsorption process obeyed the pseudo-second-order kinetic model, and the maximum adsorption capacity of AO7 was estimated to be 132 mg g⁻¹, which is much higher than the bamboo charcoal, titanium dioxide and so on. Moreover, intraparticle diffusion model indicates that the adsorption process can be divided into three stages: diffusion of the AO7 to β -CD hydrogel surface, intraparticle diffusion, establishment of the adsorption equilibrium, and the host–guest interaction between the hydrophobic naphthyl group and the cavity of β -CD plays the decisive role in the adsorption of AO7 onto β -CD hydrogel.

Keywords: Absorption; β -CD hydrogel; Azo dyes; Kinetics; Isotherms

1. Introduction

Azo dyes, as an important class of colorants, have been used in several industries including textile, paper, leather and plastics [1–3]. With increasing concerns over environmental

safety and public health, efficient strategies for removing toxic azo dyes from wastewater by the means of chemical, physical and electrochemical methods have been developed. However, adsorption over porous materials has aroused to be one of the most promising approaches for water purification

* Corresponding author.

The manuscript was written through contribution from all authors. All authors have given approval to the final version of the manuscript.

1944-3994/1944-3986 © 2017 Desalination Publications. All rights reserved.

during past decades, because of its higher efficiency, lower cost and reuse [4–7]. Acid orange 7 (AO7) is one of the most common azo dyes, which is also often employed as a model pollutant in wastewater.

Over the past decades, there has been great interest in the research of the application of β -CD-based materials for drug delivery, wastewater treatment, chiral separation, catalysis and so on, owing to its unique structural characteristics and physical–chemical properties [8,9]. β -CD is cyclic oligosaccharides consisting of seven glucose units linked by α -1,4-glycosidic linkages, which has hydrophilic external face and hydrophobic internal environment [10]. As shown in Fig. 1(c), one of the most important features of β -CD is that the internal cavity is capable of encapsulating lipophilic compounds by forming inclusion complexes through host–guest interaction of which solubilize otherwise insoluble compounds in water [11]. The Harada group has prepared a series of supramolecular assemblies using β -CD inclusion complexes with adamantly [12,13], cinnamyl [14] and azobenzene [15]. The chemical structure of AO7 is shown in Fig. 1(b), which contains a hydrophobic naphthyl group that attached to the hydrophobic cavity of β -CD.

Since β -CD exhibits a decent solubility in water, and β -CD cannot be directly used for water treatment. Thus, β -CD must be grafted onto the surfaces of insoluble substance or integrated into hydrophobic polymer. Compared with two methods, β -CD-based polymer contains more

β -CD structural unit, and can effectively improve the complexation capacity of β -CD-based materials [16–19]. To date, numerous β -CD-based polymers have been studied, the structure of β -CD-based polymers is mainly divided into three categories: graft polymer [20], linear block polymer [21] and reticulation polymer [22,23], which are shown in Fig. 2. β -CD-based reticulation polymers maintain the cavity structure, and the three-dimensional porous structures provide enhanced absorptive capacity. Among these methods, polycondensation reaction using epichlorohydrin (EPI) represents an effective method to prepare water-insoluble, crosslinked β -CD-based materials.

Herein, we aimed to explore the adsorption mechanism of β -CD-based adsorbent prepared by polycondensation reaction between β -CD and EPI. By applying theoretical adsorption kinetic and adsorption isotherm models the adsorption progress obeyed pseudo-second-order kinetic model, and the maximum adsorption capacity of AO7 was estimated to be 132 mg g^{-1} through the Sips isotherm model. Furthermore, the results also showed that the host–guest interaction between hydrophobic naphthyl group and β -CD plays a critical role in the adsorption behavior of AO7.

2. Experimental setup

2.1. Materials

β -Cyclodextrin (β -CD), AO7 sodium salt and sodium hydroxide (NaOH, AR, purity $\geq 96.0\%$) purchased from

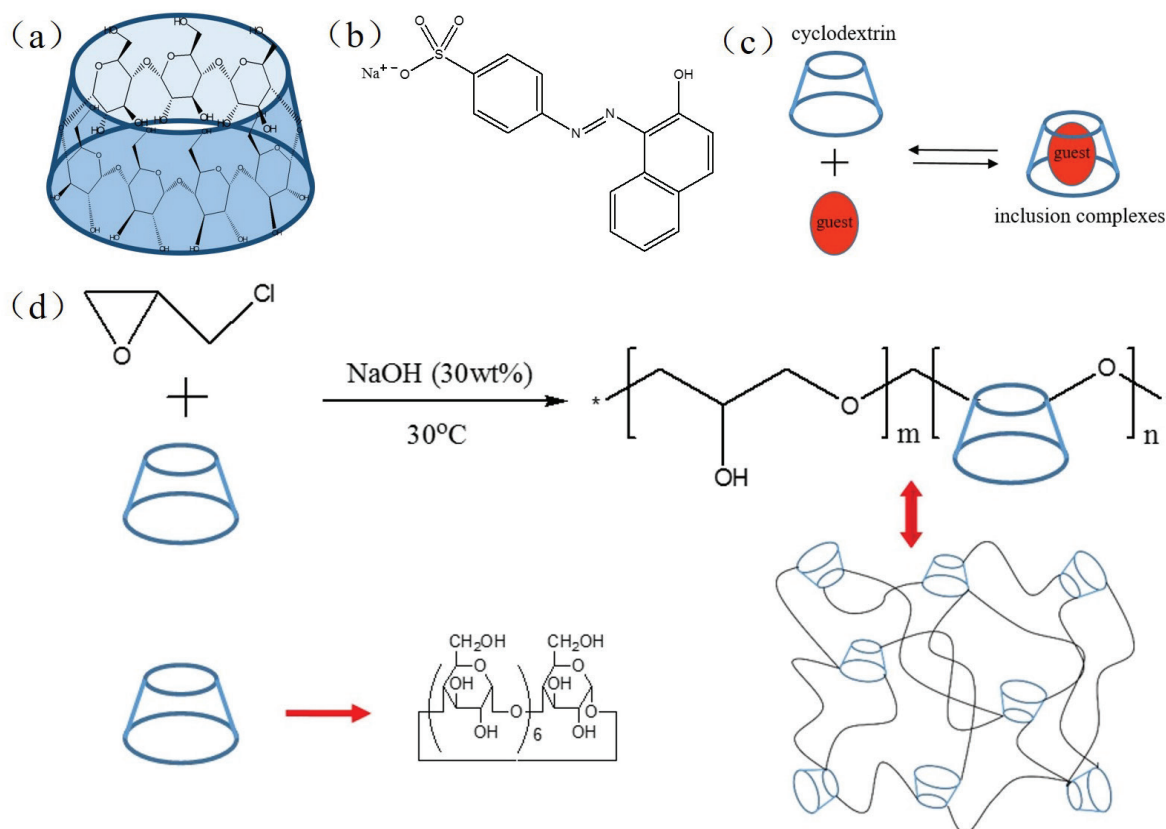


Fig. 1. The chemical structures of β -CD (a) and AO7 (b); the formation of CD inclusion complexes (c) and the preparation of β -CD hydrogel (d).

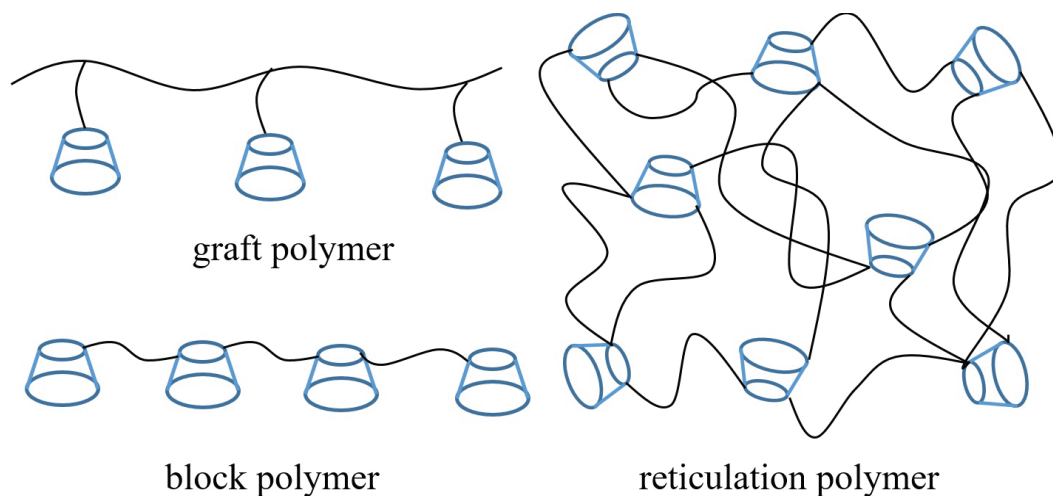


Fig. 2. The structures of β -CD-based polymer: graft polymer, block polymer and reticulation polymer.

Signopharm Chemical Reagent Co., Ltd. (Shanghai, China). EPI (AR, purity $\geq 99.0\%$) was purchased from Shanghai Ling Feng Chemical Reagent Co., Ltd. (Shanghai, China). All reagents were used directly without any purification.

2.2. Preparation of β -CD hydrogel

β -CD hydrogel was synthesized according to the similar method as previously reported [22]. Briefly, β -CD (5.00 g, 4.41 mmol) was added into a NaOH (30 wt%, 8 mL) aqueous solution. The mixture was stirred at room temperature until the solid completely dissolved. EPI (5.19 mL, 66.2 mmol) was then added dropwise to the mixture at 40°C . The reaction mixture was stirred for another 6 h at 80°C . The final product is a translucent solid gel and washed repeatedly with deionized water to remove excess NaOH and unreacted reactant. The resultant translucent gel was immersed in deionized water and the water was replaced every 6 h for 2 d. Finally, the prepared β -CD hydrogel were freeze-dried and dried in vacuum prior to use.

2.3. Characterization methods

The infrared spectra of reactants and products were obtained on a Nicolet iS50 Fourier transform infrared spectrometer (FTIR; Thermo Fisher, USA) using KBr pellets. The micrographs of β -CD hydrogel were obtained using JSM 6510LV scanning electron microscope (SEM; JEOL, Japan). The swelling ratio of β -CD hydrogel in water was measured to be 181% at room temperature.

The swelling ratio of β -CD hydrogel was determined by the following Eq. (1) [24]:

$$Q_{\text{wt}} = \frac{(W_s - W_d)}{(W_d)} \times 100\% \quad (1)$$

where Q_{wt} is the swelling ratio of β -CD hydrogel, W_s is the weight of the swollen sample at saturation (g) and W_d is the weight of the dried β -CD hydrogel.

AO7 aqueous solutions were prepared at specific concentrations ranging from 10 to 500 ppm. The maximum

absorption wavelength of AO7 aqueous solutions at about 484.5 nm was obtained on a UV–visible spectrophotometer (UV762, Shanghai, China), and selected for monitoring the adsorption process. The concentration of AO7 present in solution after the adsorption experiment was determined by UV–visible spectroscopy using a calibration curve of the absorbance vs. the concentration.

2.4. Adsorption study with AO7

A series of adsorption AO7 experiments were carried out under different conditions including temperature, initial concentration and pH. In this experiment, 30 mg dried β -CD hydrogel and 40 mL of AO7 aqueous solution were placed in 50 mL Erlenmeyer flasks, then placed in a water bath immediately.

The amount of adsorbed dye onto β -CD hydrogel was determined by the following equation:

$$q_e = \frac{(C_0 - C_e)V}{m} \quad (2)$$

where q_e is the amount of adsorbed dye at equilibrium per gram of material (mg g^{-1}); C_0 is the initial concentration of dye (mg L^{-1}) in solution; C_e is the concentration of dye on the equilibrium (mg L^{-1}); V is the volume of dye solution (L) and m is the mass of the adsorbent (g).

2.5. Adsorption kinetics and adsorption isotherm models

The experimental data of adsorbed AO7 onto β -CD hydrogel were fitted with the theoretical adsorption kinetics and isotherm models. And then, the results of simulation via different models were compared and analyzed to evaluate the adsorption kinetics and isotherm models.

In this study, the adsorption progress was fitted using pseudo-first-order [25], pseudo-second-order [26], chemisorption [27], fractionary order [28] and intraparticle diffusion models [29]. And, the equilibrium data were fitted using Freundlich [30], Langmuir [31] and Sips [32] models.

3. Results and discussion

3.1. Fourier transform infrared spectroscopy

For adsorption performance of β -CD hydrogel, the structural integrity of β -CD is a crucial factor. FTIR is an effective method to characterize the chemical structures of insoluble, crosslinked materials. Fig. 3 shows the infrared spectra of reactants and products. The characteristic peak of α -1,4-glycosidic bonds of β -CD was observed at 857 cm^{-1} , and the characteristic O–H stretching vibration peaks and CH_2 -asymmetrical stretching vibration from β -CD were observed at $3,445$ and $2,923\text{ cm}^{-1}$, respectively. The characteristic peak in the range of $1,134$ – $1,049\text{ cm}^{-1}$ is due to the C–O and C–O–C stretching. Compared with β -CD, the characteristic peak at $2,881\text{ cm}^{-1}$ of β -CD hydrogel is assigned to the C–H stretching vibration, and the change of the peak of the O–H bond is due to the relative increase of O–H after reaction. In the FTIR spectrum of dried β -CD hydrogel, however, the characteristic peak of β -CD stays same as initial β -CD. This indicates that the structure of β -CD did not change during the process

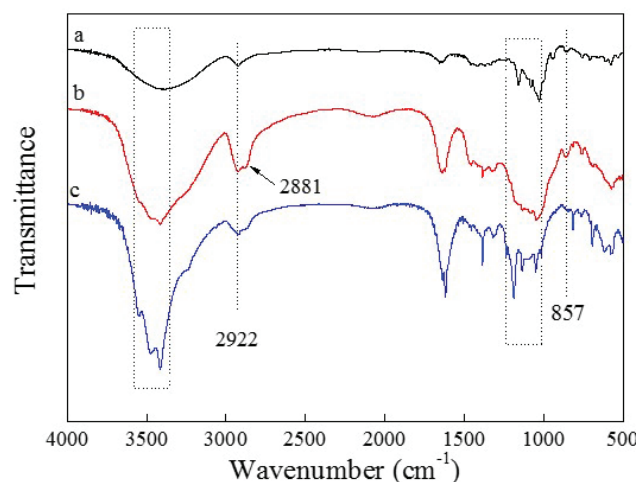


Fig. 3. The infrared spectra of reactants and products of β -CD (a), dried β -CD hydrogel (b) and dried β -CD hydrogel after adsorption (c).

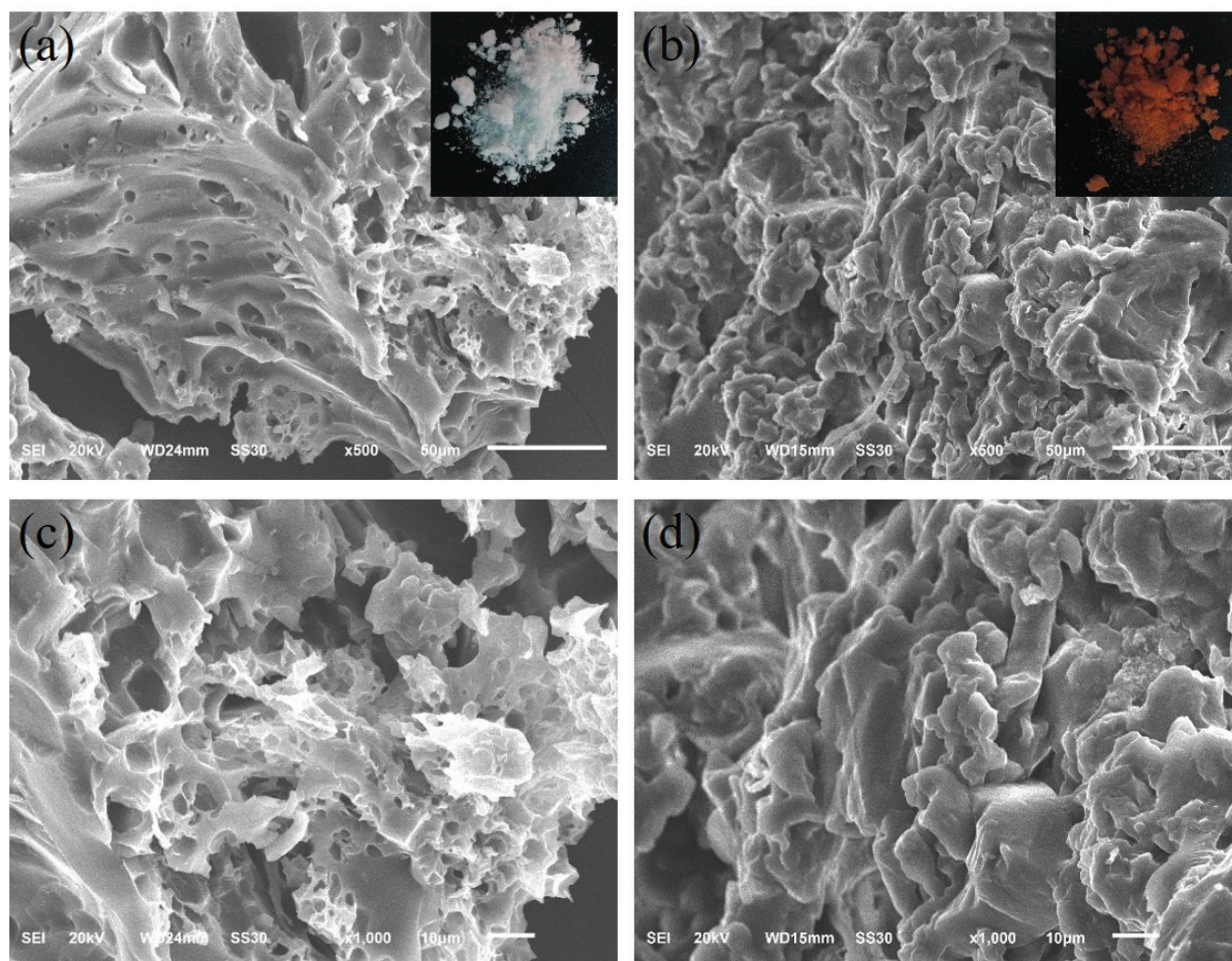


Fig. 4. SEM micrographs of β -CD hydrogel at different magnifications of β -CD hydrogel before the adsorption of AO7 (a) and (c); and β -CD hydrogel after the adsorption AO7 (b) and (d).

of preparation of β -CD hydrogel. Compared with the characteristic peak O–H of β -CD hydrogel, the split peak occur remarkably in the range of $3,550\text{--}3,416\text{ cm}^{-1}$ is due to the association (hydrogen bond) between –OH of β -CD hydrogel and --SO_3^- or –OH of AO7.

3.2. Scanning electron microscopy

SEM images of the β -CD hydrogel show distinct different microstructure before and after adsorption. Figs. 4(a) and (c) show the porosity β -CD hydrogel, which the pores are uniformly distributed in the β -CD hydrogel. And, the distribution of pore size ranges from 1 to 10 μm . However, compared with the micrographs of the initial β -CD hydrogel, we can observe that the pore is filled with AO7 from β -CD hydrogel after the adsorption AO7 (Figs. 4(b) and (d)). Furthermore, the images of the color change of the dried β -CD hydrogel before and after adsorption shown in Figs. 4(a) and (b). Therefore, it is a crucial pore structure that β -CD hydrogel can adsorb AO7.

3.3. Thermal gravimetric analysis

Thermal gravimetric analysis (TGA) of β -CD hydrogel and β -CD hydrogel/AO7 (representing the β -CD hydrogel after adsorption AO7) is shown in Fig. 5. In the TGA plot, the weight loss of β -CD hydrogel or β -CD hydrogel/AO7 can be divided into three stages, and the detailed weight loss in each step is shown in Table 1. In the first stage, the weight loss of water illustrates the property of water absorbing in β -CD hydrogel. However, the weight loss in the both second and third stages is attributed to the decomposition of β -CD hydrogel. The only difference is that the weight loss in the third stages is mainly attributed to the decomposition of crosslinking point in β -CD hydrogel. Furthermore, the initial temperature in second stage is up to 280°C indicating its high thermal stability.

3.4. Effect of the pH value

The effect of the pH value on the adsorption capacity was studied as shown in Fig. 6. Obviously, the equilibrium adsorption capacity in acidic or alkaline condition is higher than neutrality condition. β -CD hydrogel contains a large number of hydroxyl groups. In acidic condition, the hydroxyl groups combine hydrogen ions to form a positively charged group (--OH_2^+). In alkaline condition, however, the hydroxyl groups ionize to form a negatively charged group (--O^-). The microporous volume of β -CD hydrogel increases in acidic or alkaline condition owing to the electrostatic repulsion, and the equilibrium

Table 1
Weight loss of β -CD hydrogel or β -CD hydrogel/AO7

Stage	Temperature ($^\circ\text{C}$)	β -CD hydrogel (wt%)	β -CD hydrogel/AO7 (wt%)
First step	40–120	7	6
Second step	280–430	75	69
Third step	470–600	18	25

adsorption capacity increases. Furthermore, the equilibrium adsorption capacity in acidic is obviously lower than alkaline condition, because the β -CD is decomposed, partially.

3.5. Adsorption kinetic studies

Enough contact time to adsorb AO7 onto β -CD hydrogel is crucial to study the adsorption process. The adsorption kinetic experiments were executed at 298 K, in which a 30 mg sample of dried β -CD hydrogel and 40 mL of AO7 aqueous solution were placed in a 50 mL beaker. The adsorption kinetics of AO7 was monitored as a function of time by measuring the absorbance of samples. In the first 480 min, the relationship between adsorption quantity and time is shown in Fig. 7(a). The adsorption process was similar to other adsorption, which the amount of AO7 adsorption increases with the increasing of contact time or initial concentration, and the rate of adsorption decreases with the increasing of contact time and slowly reached to zero at last. Furthermore, the rate of adsorption increases with the increasing of initial concentration at the early stage of adsorption.

To study the adsorption process, the adsorption kinetic experiment was carried out at a fixed adsorbent

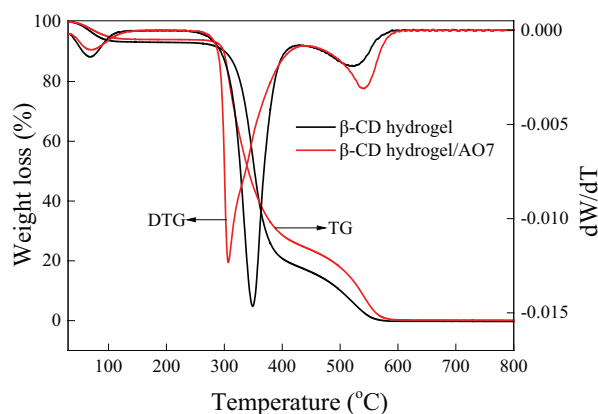


Fig. 5. TGA of β -CD hydrogel and β -CD hydrogel/AO7.

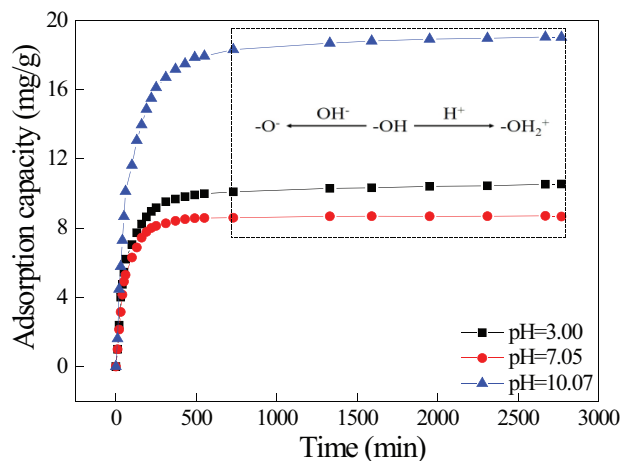


Fig. 6. Effect of the pH value on the adsorption capacity.

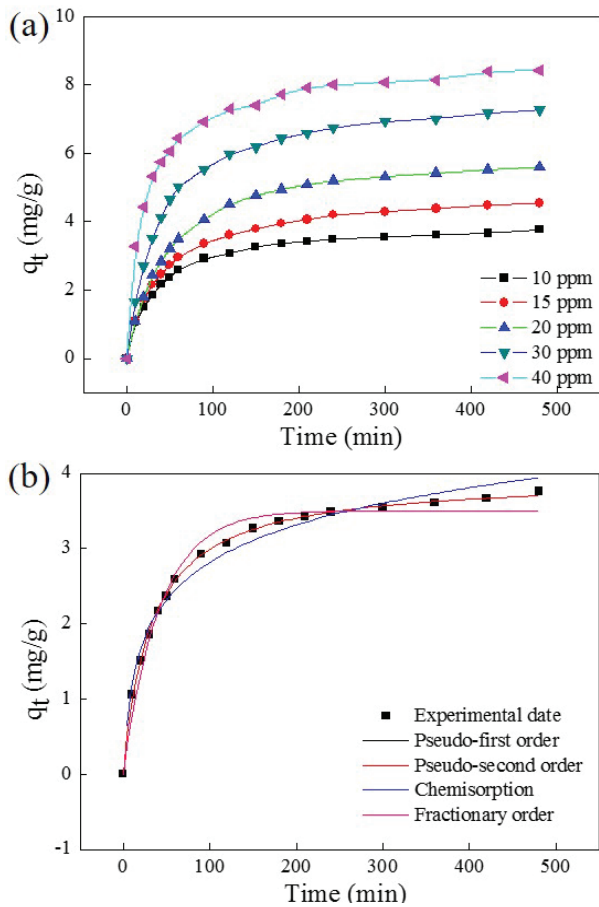


Fig. 7. Effects of contact time and initial concentration of AO7 aqueous solution on AO7 by β -CD hydrogel (a) and simulation of kinetic models of adsorbed AO7 onto β -CD hydrogel (b).

Table 2
Kinetic parameters for AO7 adsorption onto β -CD hydrogel

Kinetic model	Equation	Parameter	Data
Pseudo-first-order	$q_t = q_e [1 - e^{-(k_1 t)}]$	q_e (mg g ⁻¹)	3.51
		k_1 (min ⁻¹)	2.36×10^{-2}
		R^2	0.9784
Pseudo-second-order	$q_t = \frac{k_2 q_e^2 t}{1 + k_2 q_e t}$ $\frac{t}{q_t} = \frac{1}{k_2 q_e^2} + \frac{t}{q_e}$	q_e (mg g ⁻¹)	3.95
		k_2 (g mg ⁻¹ min ⁻¹)	7.85×10^{-3}
		R^2	0.9998
Chemisorption (Elovich)	$q_t = \frac{1}{\beta} \ln(\alpha\beta) + \frac{1}{\beta} \ln(t)$	α (mg g ⁻¹ min ⁻¹)	0.367
		β (g mg ⁻¹)	1.40
		R^2	0.9749
Fractionary order (Avrami)	$q_t = q_e [1 - e^{-(k_{AV} t)^{n_{AV}}}]$	q_e (mg g ⁻¹)	3.51
		k_{AV} (min ⁻¹)	8.46×10^{-2}
		n_{AV}	0.280
		R^2	0.9769

Note: q_e and q_t (mg g⁻¹) are the amount of adsorbed AO7 at time t and equilibrium, respectively; t (min) is the time of adsorption; k_1 and k_2 are the rate constant of pseudo-first-order and pseudo-second-order, α and β are the initial adsorption rate of Elovich model and Elovich constant, respectively; k_{AV} and n_{AV} are the Avrami kinetic constant and the fractionary reaction order (Avrami), respectively.

concentration (0.75 mg mL⁻¹) and temperature (298 K) at various initial AO7 concentrations. At the same time, the fundamental kinetic models were employed using nonlinear fitting method as shown in Fig. 7(b). And, the relevant kinetic parameters, with the initial concentration of AO7 was 10 ppm, are shown in Table 2. Obviously, the pseudo-second-order kinetic model presented the best fitting, and the correlation coefficients (R^2) varied close to 1 ($R^2 > 0.999$).

In order to verify whether the adsorption progress also obey pseudo-second-order kinetic model at different initial AO7 concentrations (from 10 to 40 ppm), the experimental data of the adsorption for AO7 onto β -CD hydrogel were fitted according to nonlinear and linear fitting method as shown in Figs. 8(a) and (b). Furthermore, the relevant pseudo-second-order kinetic parameter values of AO7 adsorption for β -CD hydrogel at different initial concentrations are shown in Table 3. k_2 is the pseudo-second-order rate constant obtained via the slope and intercept of linear pseudo-second-order equation or the parameters of nonlinear pseudo-second-order equation, and k_2 equal to the square of the slope divided by the intercept when the t/q_t was plotted against t . The amount of AO7 adsorbed at equilibrium obtained from experiment at different initial concentrations was very close to the theoretical value. And the correlation coefficients (R^2) were very close to 1 ($R^2 > 0.999$) at different initial concentrations. These results indicated that the progress of adsorbed AO7 onto β -CD hydrogel obey pseudo-second-order kinetic model under different initial concentration.

In order to thoroughly understand the different stages of adsorption process, the intraparticle diffusion model was employed to calculate the diffusion rate constant and assess the effect of resistance during the every stage of the adsorption for AO7 onto β -CD hydrogel.

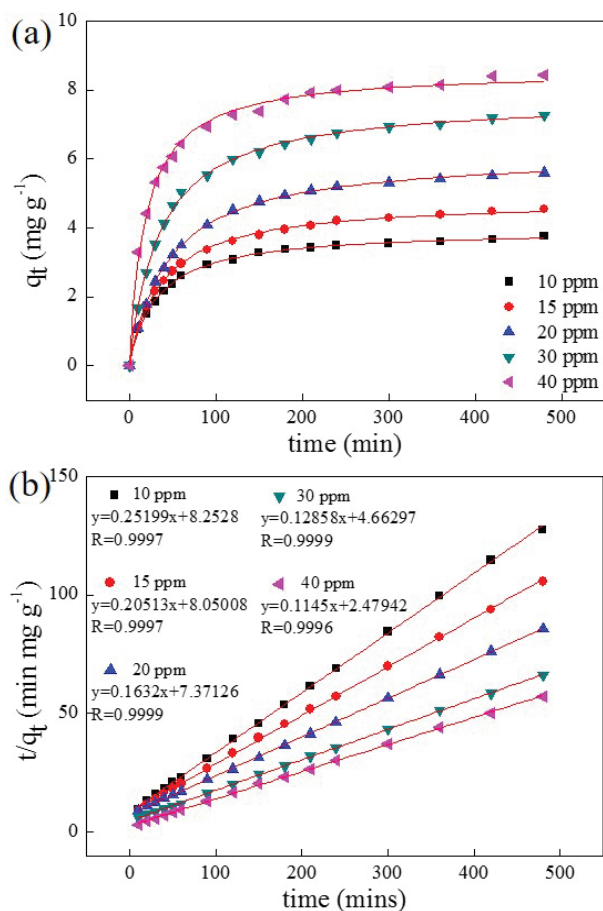


Fig. 8. Simulations of pseudo-second-order kinetic models of AO7 adsorption at different initial concentration according to nonlinear (a) and linear (b) fitting method.

Table 3
Pseudo-second-order kinetics constants for AO7 adsorption onto β -CD hydrogel

C_0 (ppm)	$q_{e(\text{exp})}$ (mg g^{-1})	$q_{e(\text{cal})}$ (mg g^{-1})	k_2 ($\text{g mg}^{-1} \text{min}^{-1}$)	R^2
10	3.764	3.951	7.853×10^{-3}	0.9997
15	4.545	4.822	5.508×10^{-3}	0.9997
20	5.595	6.163	3.523×10^{-3}	0.9999
30	7.264	7.747	3.645×10^{-3}	0.9999
40	8.423	8.567	6.168×10^{-3}	0.9996

Note: C_0 is the initial concentration of AO7 aqueous solution; $q_{e(\text{exp})}$ and $q_{e(\text{cal})}$ are the amount of adsorbed AO7 at equilibrium from the experimental measurements and the theoretical calculation, respectively.

Intraparticle diffusion model equation is shown as follows:

$$q_t = k_{\text{id}} \sqrt{t} + c \quad (3)$$

where k_{id} is the intraparticle diffusion rate constant; t (min) is the time of adsorption.

Fig. 9(a) shows the relationship between the amount of adsorbed AO7 at time t (q_t) and the square root of time ($\text{time}^{0.5}$). Through linear fitting, this adsorption process can be divided into three stages. The first stage, which can be described as AO7 diffusion process up to in solution, can be considered the faster adsorption stage, owing to the least resistance (Fig. 9(b) from A to B). In this stage, the driving force of adsorption is mainly the interaction between adsorbent and adsorbate, and the concentration difference between solution and β -CD hydrogel surface. Thus, it is noteworthy that the adsorption rate of this stage increases with the increasing initial concentration. The second stage can be described as intraparticle diffusion, which adsorption rate of this stage is slower than first stage owing to the resistance of β -CD hydrogel (Fig. 9(b) from B to C). In this stage, the driving force of adsorption is only the concentration difference between surface and intraparticle β -CD hydrogel. The last stage can be considered the establishment of the adsorption equilibrium. And, the adsorption rate of this stage is very close to zero but not equal to zero, which is due to the formation of β -CD inclusion complex with AO7 as shown in Fig. 9(b) (inset D) [33].

3.6. Equilibrium adsorption isotherms studies

Adsorption isotherm is most important data source for practical application and fundamental understanding of the β -CD-based hydrogel adsorbents. In order to gain a deeper understanding of the adsorption mechanism and the maximum adsorption capacity for AO7 of β -CD hydrogel, adsorption isothermal experiment for AO7 onto β -CD hydrogel were conducted at different initial AO7 concentrations (from 10 to 500 ppm) over 600 min at 298 K. Moreover, theoretical isotherm models were employed to study the interactive behavior between AO7 and β -CD hydrogel. The simulations of isotherm models of the adsorption for AO7 onto β -CD hydrogel according to nonlinear method are shown in Fig. 10. The relevant isotherm models parameters for AO7 adsorption onto β -CD hydrogel were shown in Table 4. By comparison, the Sips isotherm model presented the best correlation, which the value of the correlation coefficient (R^2) was up to 0.9972. This means the adsorption for AO7 adsorption onto β -CD hydrogel was multilayer adsorption at low concentrations.

4. Conclusions

In this work, β -CD hydrogel was synthesized by using EPI as an effective crosslinking agent. The adsorption behavior was investigated at various pH and dye concentration. We found that the equilibrium adsorption capacity in acidic or alkaline condition is higher than neutrality condition. The results showed that the pseudo-second-order kinetic model presented best fit to the adsorption progress compared with other theoretical kinetic models, and the isothermal adsorption was identical with Freundlich isotherm model at low temperature. The further study of adsorption mechanism showed that this β -CD hydrogel is promising to apply in water treatment.

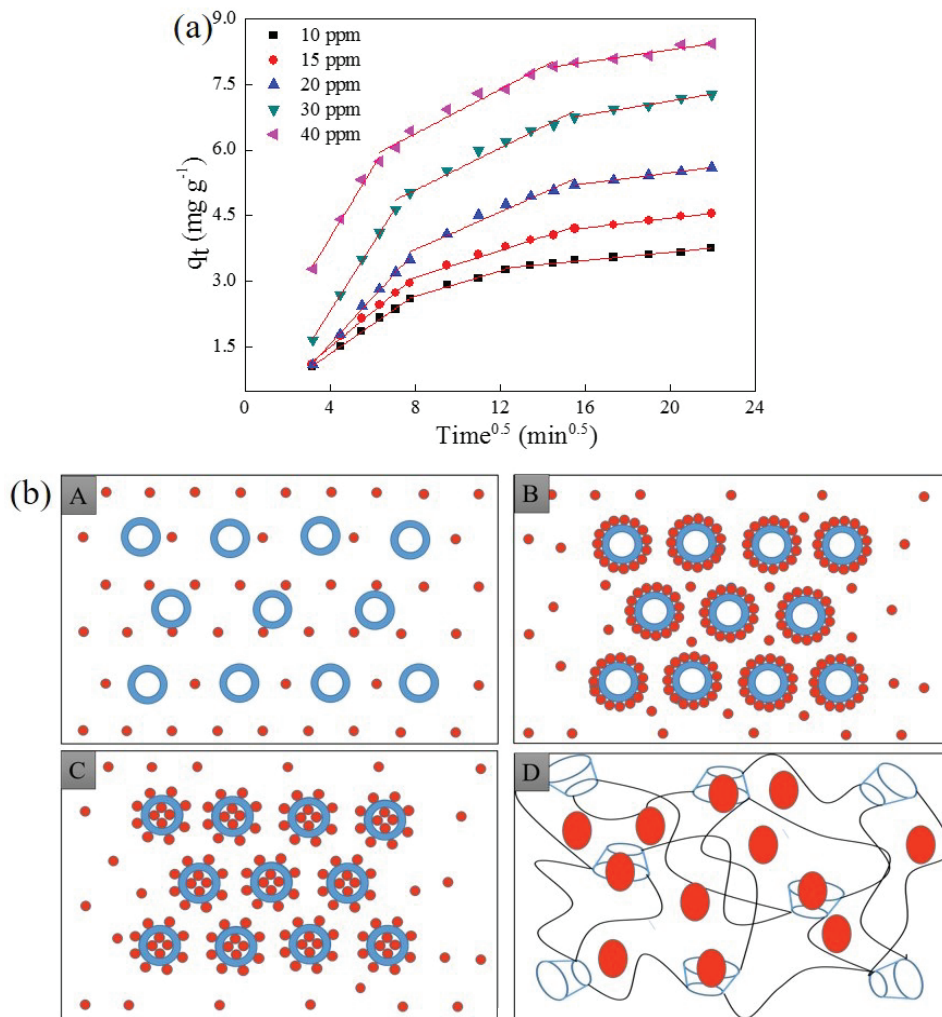


Fig. 9. Simulation of intraparticle diffusion model (a) and the illustration of adsorption process at different stage (b).

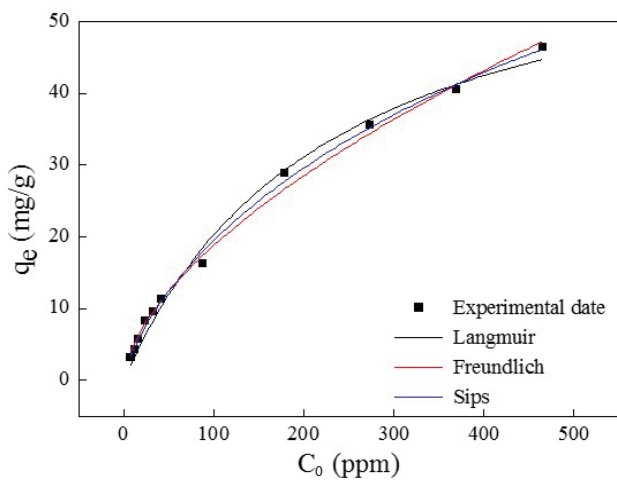


Fig. 10. Adsorption isotherms of AO7 for β-CD hydrogel from aqueous solutions and simulations obtained using theoretical isotherm models.

Table 4
Isotherm parameters for AO7 adsorption onto β-CD hydrogel

Isotherm model	Equation	Parameter	Data
Langmuir	$q_e = \frac{q_s K_L C_e}{1 + K_L C_e}$	q_s (mg g ⁻¹)	66.73
		K_L (L mg ⁻¹)	4.380×10^{-2}
		R^2	0.9913
Freundlich	$q_e = K_F C_e^{1/n_F}$	K_F (mg g ⁻¹)	1.198
		$(L \text{ mg}^{-1})^n$	
		n_F	1.672
Sips	$q_e = \frac{q_s K_S C_e^{1/n_s}}{1 + K_S C_e^{1/n_s}}$	q_s (mg g ⁻¹)	131.6
		K_S (L mg ⁻¹)	5.860×10^{-3}
		n_s	1.358
		R^2	0.9972

Note: q_e and q_s (mg g⁻¹) are the amount of adsorbed AO7 at equilibrium and the theoretical saturation capacity, respectively; C_e is the concentration of AO7 at equilibrium; K_L is the constant of Langmuir model; K_F and n_F are the constant and exponent of Freundlich model, respectively; K_S and n_s are the constant and exponent of Sips model, respectively.

Acknowledgments

This study has been supported by the National High Technology Research and Development Program (863 program) of China No. 2012AA06A111; Hubei Provincial Natural Science Foundation of China No. 2014CFB552; Hubei Collaborative Innovation Center for Advanced Organic Chemical Materials of China No. 000-01647909.

References

- [1] E. Clonfero, P. Venier, M. Granella, A.G. Levis, Leather azo dyes: mutagenic and carcinogenic risks, *Med. Lav.*, 81 (1990) 222–229.
- [2] L.C. Abbott, P. Macfaul, L. Jansen, J. Oakes, J.R.L. Smith, J.N. Moore, Spectroscopic and photochemical studies of xanthene and azo dyes on surfaces: cellophane as a mimic of paper and cotton, *Dyes Pigm.*, 48 (2001) 49–56.
- [3] R. Ansari, Z. Mosayebzadeh, Application of polyaniline as an efficient and novel adsorbent for azo dyes removal from textile wastewaters, *Chem. Pap.*, 65 (2010) 1–8.
- [4] L. Li, Z. Shi, H. Zhu, W. Hong, F. Xie, K. Sun, Adsorption of azo dyes from aqueous solution by the hybrid MOFs/GO, *Water Sci. Technol.* 73 (2016) 1728–1737.
- [5] G. Jingqun, J. Renzheng, W. Jun, K. Pingli, W. Baoxin, L. Ying, L. Kai, Z. Xiangdong, The investigation of sonocatalytic activity of Er^{3+} : $\text{YAlO}_3/\text{TiO}_2$ -ZnO composite in azo dyes degradation, *Ultrason. Sonochem.*, 18 (2011) 541–548.
- [6] N. Sahu, K.M. Parida, Photocatalytic activity of Au/TiO_2 nanocomposite for azo-dyes degradation, *Kinet. Catal.*, 53 (2012) 197–205.
- [7] D. Vaněrková, A. Sakalis, M. Holčápek, P. Jandera, A. Voulgaropoulos, Analysis of electrochemical degradation products of sulphonated azo dyes using high-performance liquid chromatography/tandem mass spectrometry, *Rapid Commun. Mass Spectrom.*, 20 (2006) 2807–2815.
- [8] J.W. Zhou, H. Ritter, Cyclodextrin functionalized polymers as drug delivery systems, *J. Polym. Sci., Part A: Polym. Chem.*, 1 (2010) 1552–1559.
- [9] F. van de Manakker, T. Vermonden, C.F. van Nostrum, W.E. Hennink, Cyclodextrin-based polymeric materials: synthesis, properties, and pharmaceutical/biomedical applications, *Biomacromolecules*, 10 (2009) 3157–3175.
- [10] K. Freudenberg, E. Schaaf, G. Dumpert, T. Ploetz, Neue Ansichten über die Stärke, *Sci. Nature*, 27 (1939) 850–853.
- [11] G. Chen, M. Jiang, Cyclodextrin-based inclusion complexation bridging supramolecular chemistry and macromolecular self-assembly, *Chem. Soc. Rev.*, 40 (2011) 2254–2266.
- [12] A. Miyawaki, M. Miyauchi, Y. Takashima, H. Yamaguchi, A. Harada, Formation of supramolecular isomers; poly[2]rotaxane and supramolecular assembly, *Chem. Commun.*, 4 (2008) 456–458.
- [13] K. Miyamae, M. Nakahata, Y. Takashima, A. Harada, Self-healing, expansion–contraction, and shape-memory properties of a preorganized supramolecular hydrogel through host–guest interactions, *Angew. Chem. Int. Ed.*, 127 (2015) 8984–8987.
- [14] M. Miyauchi, A. Harada, Construction of supramolecular polymers with alternating α -, β -cyclodextrin units using conformational change induced by competitive guests, *J. Am. Chem. Soc.*, 126 (2004) 11418–11419.
- [15] A. Harada, A. Hashidzume, Y. Takashima, Cyclodextrin-based supramolecular polymers, *Chem. Soc. Rev.*, 38 (2009) 1–43.
- [16] E.Y. Ozmen, M. Sezgin, A. Yilmaz, M. Yilmaz, Synthesis of beta-cyclodextrin and starch based polymers for sorption of azo dyes from aqueous solutions, *Bioresour. Technol.*, 99 (2008) 526–531.
- [17] E. Yilmaz, S. Memon, M. Yilmaz, Removal of direct azo dyes and aromatic amines from aqueous solutions using two beta-cyclodextrin-based polymers, *J. Hazard. Mater.*, 174 (2010) 592–597.
- [18] M. Arslan, S. Sayin, M. Yilmaz, Removal of carcinogenic azo dyes from water by new cyclodextrin-immobilized iron oxide magnetic nanoparticles, *Water Air Soil Pollut.*, 224 (2013) 1527.
- [19] A. Alsaibee, B.J. Smith, L. Xiao, Y. Ling, D.E. Helbling, W.R. Dichtel, Rapid removal of organic micropollutants from water by a porous beta-cyclodextrin polymer, *Nature*, 529 (2016) 190–194.
- [20] P. Yuan, L. Chengde, Z. Zhongxing, L. Kerh Li, C. Jianhai, L. Jun, Chitosan-*graft*-(PEI- β -cyclodextrin) copolymers and their supramolecular PEGylation for DNA and siRNA delivery, *Biomaterials*, 32 (2011) 8328–8341.
- [21] E. Renard, G. Volet, C. Amiel, Synthesis of a novel linear water-soluble β -cyclodextrin polymer, *Polym. Int.*, 54 (2005) 594–599.
- [22] E. Renard, B. Seville, G. Barnathan, A. Deratani, Polycondensation of cyclodextrins with epichlorohydrin. Influence of reaction conditions on the polymer structure, *Macromol. Symp.*, 122 (1997) 229–234.
- [23] N. Morin-Crini, G. Crini, Environmental applications of water-insoluble β -cyclodextrin–epichlorohydrin polymers, *Prog. Polym. Sci.*, 38 (2013) 344–368.
- [24] A.I. Panou, K.G. Papadokostaki, P.A. Tarantili, M. Sanopoulou, Effect of hydrophilic inclusions on PDMS crosslinking reaction and its interrelation with mechanical and water sorption properties of cured films, *Eur. Polym. J.*, 49 (2013) 1803–1810.
- [25] S. Lagergren, Zur Theorie der sogenannten Absorption gelöster Stoffe, *PA Norstedt & söner*, 1898.
- [26] Y.S. Ho, G. McKay, Pseudo-second order model for sorption processes, *Process Biochem.*, 34 (1999) 451–465.
- [27] S.Y. Elovich, G. Zhabrova, Mechanism of the catalytic hydrogenation of ethylene on nickel: I. Kinetics of the process, *J. Phys. Chem.*, 13 (1939) 1761–1775.
- [28] N.F. Cardoso, E.C. Lima, I.S. Pinto, C.V. Amavisca, R. Betina, R.B. Pinto, W.S. Alencar, S.F.P. Pereira, Application of cupuassu shell as biosorbent for the removal of textile dyes from aqueous solution, *J. Environ. Manage.*, 92 (2011) 1237–1247.
- [29] W.J. Weber, J.C. Morris, Kinetics of adsorption on carbon from solution, *J. Sanit. Eng. Div.*, 89 (1963) 31–60.
- [30] H. Freundlich, Over the adsorption in solution, *J. Phys. Chem.*, 57 (1906) e470.
- [31] I. Langmuir, The constitution and fundamental properties of solids and liquids. Part II—liquids, *J. Am. Chem. Soc.*, 38 (1915) 102–105.
- [32] R. Sips, On the structure of a catalyst surface, *J. Chem. Phys.*, 16 (1948) 1024–1026.
- [33] D.Y. Pratt, L.D. Wilson, J.A. Kozinski, A.M. Mohart, Preparation and sorption studies of beta-cyclodextrin/epichlorohydrin copolymers, *J. Appl. Polym. Sci.*, 116 (2010) 2982–2989.